Published in final edited form as:
Atmosphere (Basel). 2020 ; 11(12): . doi:10.3390/atmos11121289.

Data assimilation of ambient concentrations of multiple air pollutants using an emission-concentration response modeling framework

Jia Xing[1,2,†], **Siwei Li**[3,4,†,*], **Dian Ding**[1,2], **James T. Kelly**[5], **Shuxiao Wang**[1,2,*], **Carey Jang**[5], **Yun Zhu**[6], **Jiming Hao**[1,2]

[1]State Key Joint Laboratory of Environmental Simulation and Pollution Control, School of Environment, Tsinghua University, Beijing 100084, China

[2]State Environmental Protection Key Laboratory of Sources and Control of Air Pollution Complex, Beijing 100084, China

[3]School of Remote Sensing and Information Engineering, Wuhan University, Wuhan 430079, China

[4]State Key Laboratory of Information Engineering in Surveying, Mapping and Remote Sensing, Wuhan University, Wuhan 430079, China

[5]Office of Air Quality Planning and Standards, U.S. Environmental Protection Agency, Research Triangle Park, NC 27711, USA

[6]College of Environment and Energy, South China University of Technology, Guangzhou Higher Education Mega Center, Guangzhou 510006, China

Abstract

Data assimilation for multiple air pollutant concentrations has become an important need for modeling air quality attainment, human exposure and related health impacts, especially in China that experiences both $PM_{2.5}$ and O_3 pollution. Traditional data assimilation or fusion methods are mainly focused on individual pollutants, and thus cannot support simultaneous assimilation for both $PM_{2.5}$ and O_3. To fill the gap, this study proposed a novel multipollutant assimilation method by using an emission-concentration response model (noted as RSM-assimilation). The new method was successfully applied to assimilate precursors for $PM_{2.5}$ and O_3 in the 28 cities of the North China Plain (NCP). By adjusting emissions of five pollutants (i.e., NO_x, SO_2, NH_3, VOC and primary $PM_{2.5}$) in the 28 cities through RSM-assimilation, the RMSEs (root mean square errors) of O_3 and $PM_{2.5}$ were reduced by about 35% and 58% from the original simulations. The

*Corresponding Authors: Siwei Li (siwei.li@whu.edu.cn); Shuxiao Wang (shxwang@tsinghua.edu.cn).
†These authors contributed equally to this study.

Author Contributions: Conceptualization, methodology, validation, formal analysis, and original draft preparation—J.X. and S.L.; resources, D.D. and Y.Z.; data curation, S.W.; writing—review and editing, J.K.; supervision, project administration, and funding acquisition—S.W., CJ, and JH; All authors have read and agreed to the published version of the manuscript.

Conflicts of Interest: The authors declare no conflict of interest. The funders had no role in the design of the study; in the collection, analyses, or interpretation of data; in the writing of the manuscript, or in the decision to publish the results.

RSM-assimilation results small sensitivity to the number of observation sites due to the use of prior knowledge of the spatial distribution of emissions; however, the ability to assimilate concentrations at the edge of the control region is limited. The emission ratios of five pollutants were simultaneously adjusted during the RSM-assimilation, indicating that the emission inventory may underestimate NO_2 in January, April and October, and SO_2 in April, but overestimate NH_3 in April and VOC in January and October. Primary $PM_{2.5}$ emissions are also significantly underestimated, particularly in April (dust season in NCP). Future work should focus on expanding the control area and including NH_3 observations to improve the RSM-assimilation performance and emission inventories.

Keywords

data assimilation; response model; ozone; $PM_{2.5}$; emission inversion

1. Introduction

Human exposure to air pollutants such as ozone (O_3) and fine particulate matter ($PM_{2.5}$) has been associated with considerable adverse health effects. In 2017, 2.9 million premature mortalities were attributed to $PM_{2.5}$ exposure globally and about a half-million mortalities were attributed to O_3 exposure [1–2]. Accurate estimation of air pollutant concentrations and their exposures is critical for assessing health impacts and developing emission control strategies. Previous studies have demonstrated that the assimilation of chemical transport model (CTM) simulations with monitor observations can provide spatiotemporally continuous estimates of air pollutant concentrations and corresponding exposure while incorporating the accuracy of in-situ monitoring data and the spatiotemporal continuity of CTM modeling. Traditional data fusion methods such as Voronoi Neighbor Averaging (VNA) [3], enhanced Voronoi Neighbor Averaging (eVNA) [4], and Downscaler (DS) [5–6] have been applied in many studies to estimate air pollutant concentrations, human exposure and related health impacts [7]. Concentration estimates based on fusing monitor and CTM data can be helpful in characterizing the effects of control strategies for air quality attainment [8].

However, traditional data fusion is mostly based on statistical interpolation or regression methods that are designed to predict each pollutant individually. The need for simultaneous assimilation of multiple pollutants is evident with the deterioration of O_3 pollution in China corresponding to $PM_{2.5}$ improvements [9]. The challenge for multipollutant assimilation is to wisely design certain constraints to maintain the natural linkages between pollutants during the assimilation process. Specifically, the natural linkage between O_3 and $PM_{2.5}$ is that both pollutants have contributions from common precursors (NO_x and VOC), similar atmospheric diffusion/advection transport, and chemical oxidation reactions. Therefore the modulation of one pollutant concentration should exert corresponding influence on the other, and these connections should be represented during the assimilation. Traditional data fusion methods like eVNA can only fuse pollutant concentrations separately without considering multipollutant linkages. However, assimilating O_3 and $PM_{2.5}$ separately will result in different NO_x and VOC adjustment ratios since the optimization is conducted individually

for one pollutant instead of both. The simultaneous assimilation for both pollutants can result in a consistent adjustment of NO_x and VOC emissions and also provide additional constraints to ensure the inversion problem is well posed [10]. Therefore, the development of an advanced data assimilation method is necessary to support simultaneous data fusion for multiple pollutants to accurately represent current air quality and the effectiveness of future control policies.

Discrepancies between predictions and observations are associated with uncertainties in many factors such as model emissions, resolution, chemical mechanisms, and process parameterizations as well as measurement errors. Among these factors, uncertainties in emission inventories are regarded as one of the largest contributors to the biases in CTM predictions. Unfortunately, the interpolation-based fusion methods like eVNA do not provide information on the contributors to model errors. Inversion modeling studies have used advanced assimilation techniques such as ensemble Kalman filtering to correct the emissions simultaneously during the assimilation process [11]. The revised emissions are also useful for improving emission inventories [12–13]. Ideally, the predictions developed by combining CTM simulations and observations would provide not only accurate and spatiotemporally continuous concentrations of multiple pollutants, but also corrections to emission inventories, which are one of the largest contributors to model biases. To date, however, most inversion studies only focused on individual pollutants that can be measured directly. Therefore, there remains a lack of inverse emissions estimates for multiple pollutants including those that cannot be directly observed, such as primary fine particulate matter (noted as $pPM_{2.5}$).

The recently developed response surface model (RSM) provides real-time prediction of both $PM_{2.5}$ and O_3 using emission-concentration relationships. The RSM can identify the emission control factors needed to meet air quality targets, and thus provides information on the changes in emissions of multiple pollutants needed to improve air quality predictions against monitoring data [14–15]. Advanced machine learning techniques enables its fast application across any time period and spatial location [16]. Different from inversion modeling, the RSM modifies anthropogenic emissions of five pollutants at the regionally aggregated level (by city in this study) based on an assumption that the spatial distribution of emissions is relatively accurate compared with emission magnitudes. In combination with surface observations from a few monitoring sites, the RSM has been successfully applied to investigate the emission changes during the COVID-19 period in North China Plain (NCP) [17]. The RSM-based assimilation can well maintain the inner linkages of $PM_{2.5}$ and O_3, as the RSM prediction can be considered as one CTM simulation under a specific emission scenario. The emission adjustment ratios from the RSM-assimilation also address the question of how emissions should be modified to achieve a certain level of agreement between predictions and observations.

In this study, an emission-concentration response modeling framework is established based on the RSM (noted as RSM-assimilation). Then its performance in the data assimilation of ambient concentrations of multiple air pollutants is tested in the case study of NCP. The new RSM-assimilation method is described in Section 2. The performance of the RSM-assimilation approach as well as the implications for improving the emission inventory is

discussed in Section 3. Advantages, limitations and future work on RSM-assimilation are summarized in Section 4.

2. Methods

2.1. Simulation and observation data

The principle of RSM-assimilation is to nudge the CTM simulation toward available observations by adjusting the emissions. The CTM used in this study is the Community Multiscale Air Quality (CMAQ, version 5.2.1, www.epa.gov/cmaq) model, and the meteorological fields are based on a simulation with the Weather Research and Forecasting (WRF, version 3.8) model. The same configuration of WRF-CMAQ was applied as in our previous studies [18]. The Morrison double-moment microphysics scheme [19], the Rapid Radiative Transfer Model [20], Kain-Fritsch cumulus cloud parameterization [21], Pleim-Xiu land-surface physics scheme [22], and the Asymmetric Convective Model for the planetary boundary layer (PBL) physics scheme [23] were used in WRF simulation. We used the Carbon Bond 6 [24] and the AERO6 aerosol module [25] for gas-phase and particulate matter chemical mechanisms, respectively.

The simulation domain covers the 28 key cities in NCP, as shown in Figure 1. The simulations of the 27 km × 27km China domain provide the boundary conditions for the simulation of the nested domain of 9km × 9km over NCP. The anthropogenic emissions of 28 cities are based on the Multi-resolution Emission Inventory for China (MEIC) dataset for the year of 2016 [26], because the data for 2017 was not available when we initiated this work. The emissions include five major sectors, i.e., industry, power, residential, transportation, and agriculture. The gridded emissions of five air pollutants over 28 cities in NCP are shown in Figure S1. Biogenic emissions were generated by the Model for Emissions of Gases and Aerosols from Nature (MEGAN) version 2.0 [27]. The inline dust model was used to estimate the wind-blown dust emissions in the 27km × 27km China domain. Considering the wind-blown dust mostly comes from outside of NCP, we turned off the inline dust model for the simulation of 9km × 9km over NCP to reduce the computational burden associated with the RSM model development. The performance of the WRF-CMAQ model in simulating meteorological variables and pollutant concentrations was evaluated by comparing with surface observations [28]. The WRF-CMAQ model well reproduces the observed meteorology, with mean biases within ±0.5° for 2-meter temperature, ±1g/kg for 2-meter humidity, ±0.5m/s for 10-meter wind speed, and 10° for wind direction. The model also exhibits acceptable performance in simulating $PM_{2.5}$ and O_3 concentrations, with slight low-biases in $PM_{2.5}$ and high-biases in O_3. Such biases can be reduced through the data assimilation with RSM, as discussed in the Section 3.1.

The RSM model was developed based on 21 emission-control scenario simulations with the WRF-CMAQ model by implementing polynomial functions to represent the response of O_3 and $PM_{2.5}$ to emission changes of five pollutants including SO_2, NOx, VOC, NH_3 and $pPM_{2.5}$ in 28 cities in NCP [14–15]. The polynomial functions of O_3 and $PM_{2.5}$ response to emissions are shown as E1–2.

$$\Delta\ PM_{2.5} = a_1E_{NOx}^4 + a_2E_{NOx}^3 + a_3E_{NOx}^2 + a_4E_{NOx} + a_5E_{NOx}E_{NH3} + a_6E_{NOx}^4E_{VOCs} + a_7E_{NOx}^2E_{VOCs} + a_8E_{NOx}E_{VOCs} + a_9E_{SO2} + a_{10}E_{NH3}^3 + a_{11}E_{NH3}^2 + a_{12}E_{NH3} + a_{13}E_{VOCs}^2 + a_{14}E_{VOCs} + a_{15}E_{pPM2.5} \quad \text{(E1)}$$

$$\Delta\ O_3 = a_1E_{NOx}^5 + a_2E_{NOx}^4 + a_3E_{NOx}^3 + a_4E_{NOx}^2 + a_5E_{NOx} + a_6E_{NOx}^5E_{VOCs} + a_7E_{NOx}^2E_{VOCs} + a_8E_{NOx}E_{VOCs} + a_9E_{NOx}E_{VOCs}^3 + a_{10}E_{SO2} + a_{11}E_{NH3} + a_{12}E_{VOCs} + a_{13}E_{VOCs}^2 + a_{14}E_{VOCs}^3 + a_{15}E_{pPM2.5} \quad \text{(E2)}$$

where $\Delta\ O_3$ and $\Delta\ PM_{2.5}$ is the response of O_3 and $PM_{2.5}$ concentrations (i.e., change to the baseline concentration), respectively, at each simulated grid cell; E_{NOx}, E_{SO2}, E_{NH3}, E_{VOCs}, and $E_{pPM2.5}$ is the change ratio of NO_x, SO_2, NH_3, VOCs, and $pPM_{2.5}$ emissions, respectively, relative to baseline (i.e., baseline = 0); a_i is the coefficient of term i which is determined by fitting with 21 emission-control scenario simulations.

The RSM can predict O_3 and $PM_{2.5}$ responses to emission changes in good agreement with CMAQ predictions, as the out-of-sample validation of RSM predictions against CMAQ simulations yields NMBs (Normalized Mean Biases) within ±1% [28].

We gathered the observed NO_2, SO_2, O_3 and $PM_{2.5}$ measurements from monitoring sites in the 28 NCP cities from the China National Environmental Monitoring Centre (http://www.cnemc.cn/en/) (Figure 1). The daily maximum 8-hour O_3 and daily averaged $PM_{2.5}$ concentrations were assimilated for the modeling domain with 9-km horizontal grid spacing. The simulation period is January, April, July and October in 2017 to represent winter, spring, summer and fall, respectively. Assimilation performance was evaluated using the Root Mean Square Error (RMSE), Normalized Mean Bias (NMB) and R-squared (R^2).

In the baseline case of RSM-assimilation, we included all observation sites during the assimilation. To compare with the simulation, we averaged observations from sites within the same model grid cell (9km ×9km). This resulted in about 85 sites (the number is smaller than that shown in Figure 1) across 28 cities to be used in data assimilation. The monitoring sites are mostly located at the urban center of each city, were both local emission sources and regional contributions influence the ambient $PM_{2.5}$ and O_3 concentrations [29–30]. The RSM-assimilation can account for both local formation and regional transport since it was original built from CMAQ model simulations. Details about the numbers of sites used for nudging in each city are summarized in Table S1. Additionally, we designed single-site cases for each of the 28 cities in which only a single randomly-selected site was assimilated for each city. These cases were used to examine the sensitivity of the RSM-assimilation method to the number of observation sites.

2.2. RSM-assimilation framework

Figure 2 presents the framework for the newly developed RSM-assimilation method. As in our previous study [17], we first estimate the adjusted emission ratios of NO_x and SO_2 based

on the comparison of simulated and observed NO_2 and SO_2 concentrations. Next, an optimization process is implemented that samples VOC emission ratios as inputs for the RSM-O_3 model. This process results in optimized VOC emission ratios for the 28 cities that yield the best agreement between simulated and observed O_3 concentrations at the monitoring sites (determined by the average RMSE over all sites). A similar optimization process is then applied for $PM_{2.5}$, where the adjusted NO_x, SO_2 and VOC emission ratios are introduced into the RSM-$PM_{2.5}$ model and emission ratios are sampled for NH_3 and $pPM_{2.5}$ in the 28 cities. Since direct observations of surface NH_3 concentrations are unavailable, the optimized $pPM_{2.5}$ and NH_3 emission ratios correspond to the assimilated $PM_{2.5}$ concentrations that agree most closely with observed $PM_{2.5}$ concentrations among all possible combinations of emission ratios. The optimization was conducted through a multiple looping process to select the best combination of emission ratios (with a small step of 0.05) for different pollutants and cities to achieve the best overall agreement. As currently designed, the RSM is suitable for emission ratios of gas pollutants that range from 0 (fully controlled emissions) to 2 (doubled emissions). The response functions of O_3 and $PM_{2.5}$ to emission changes of gaseous precursors were fitted through the regression of multiple emission-control scenario simulations (emission ratios from 0–2); thus, the uncertainties of the response functions will be considerably larger when the emissions vary outside of the 0–2 emission ratio range. Here, we limit the adjusted emission ratios of NO_2, SO_2, VOC, and NH_3 to range from 0.1 (90% reduction) to 2.0 (100% increase). We allow a wider range for $pPM_{2.5}$ emission ratios due to the large uncertainties in $pPM_{2.5}$ emissions, particularly for fugitive emission sources like wind-blown dust. Unlike the gas pollutants, the RSM has no limits on the adjusted emission ratios for $pPM_{2.5}$, since impacts of these emissions are represented linearly in the RSM [15].

3. Results

3.1. Performance of RSM-assimilation

In Figure 3 and 4, the assimilated O_3 and $PM_{2.5}$ concentrations in the baseline RSM-assimilation case are compared with the original CMAQ simulations in terms of the spatial pattern of monthly averaged concentrations and with observations in terms of daily paired values for sites in the 28 cities. The assimilated spatial fields generally maintain the spatial distribution of the original CMAQ simulation, but have slightly modulated concentrations in areas surrounding the observation sites that better reflect observed values. The accuracy of both O_3 and $PM_{2.5}$ concentrations is enhanced through the RSM-assimilation that reduces the RMSE from 12.7–24.4 ppb (pre-assimilation) to 9.9–18.1 ppb (post-assimilation) for O_3, and from 23.7–85.3 μg m^{-3} (pre-assimilation) to 11.8–46.5 μg m^{-3} (post-assimilation) for $PM_{2.5}$.

The high biases in simulated O_3 are greatly reduced through RSM-assimilation, as the NMBs decrease from up to 50% in CMAQ to within 20% in RSM-assimilation. The underestimation of $PM_{2.5}$ is also mitigated through RSM-assimilation, as the NMBs for $PM_{2.5}$ are reduced to 0%. The comparison of daily paired predictions and observations indicates large improvements for R^2 in RSM-assimilation: e.g., the R^2 for $PM_{2.5}$ predictions increased from 0.2–0.5 (pre-assimilation) to 0.7–0.9 (post-assimilation). However, the RSM-

assimilation is much more effective for $PM_{2.5}$ than for O_3. This behavior might be associated with the large contributions to O_3 from sources that cannot be adjusted through RSM assimilation (e.g., biogenic sources) and the effectiveness of primary $PM_{2.5}$ emissions for modulating $PM_{2.5}$ concentrations. We note that the observations displayed in Figure 4 are distributed in discrete locations across the domain, and do not necessarily match the location of the simulated and assimilated concentrations (see Figure S2 for the matched location comparisons).

Time-series comparisons for O_3 and $PM_{2.5}$ in the 28 cities (Figure S3 and S4, respectively) suggest similar levels of improvement, as the RMSE was reduced after the four-month assimilation across the 28 cities.

Although the RSM-assimilation improves the simulation accuracy, large discrepancies in the performance improvements are evident among the 28 cities. To further investigate the variation of RSM-assimilation performance across all observation sites, we compared the RMSEs of CMAQ-simulated and RSM-assimilated O_3 and $PM_{2.5}$ in the 28 cities at the four-month averaged level, as shown in Figure 5.

In general, the RSM-assimilation is less effective in reducing the RMSE for sites in cities at the edge of the control region (i.e., the full 28-city area). The smallest O_3 improvements occurred in cities such as ZB on the eastern edge of the control region and YQ on the western edge of the control region. These cities had relatively large RMSEs after the assimilation, with RMSE reductions of only 6% (ZB) and −3% (YQ) (slightly worse performance) relative to the CMAQ simulation. For the other cities, the O_3 improvements are much greater, with RMSE reductions of at least 16%. For $PM_{2.5}$, YQ also has the smallest improvement, with a 24% reduction in RMSE (compared to a 50–80% for the other cities). Such results indicate that the RSM-assimilation has limited ability to improve the accuracy of concentrations at the edge of the control region, where the influence of emissions from outside of the control region is large. Enlarging the control area or combining with an RSM model based on the larger domain is recommended to improve the ability of RSM-assimilation for those cities. Meanwhile, discrepancies also exist within a city—e.g., RMSE was reduced in eastern Tianjin but increased in western Tianjin in Jan. This behavior occurs because the RSM-assimilation adjusts emissions at the city averaged level and maintains the spatial distribution of emissions within each city at the a priori estimate. Future improvement of the spatial distribution of the emission within the city is also recommended by adopting additional observations like satellites and advanced technologies like machine-learning to address such limits.

3.2 Sensitivity of RSM-assimilation to the site number

For traditional model-observation fusion methods, the abundance of observations has significant impacts on model performance [8]. However, in RSM-assimilation, the adjustment of emissions is done at the city-level, and therefore decreasing the number of observations within each city should have relatively less influence on performance compared to regression-based methods. To investigate the sensitivity of RSM performance to the number of sites used in assimilation, we examined performance for cases based on different numbers of observation sites, as shown in Figure 6.

In assimilation for the baseline case (red hollow bar), all observation sites were used. For the other cases (C1 to C3, red symbols), a single site in each city was used based on three random site selections. Compared to the baseline RSM, the performance does not decrease considerably for the single-site RSM-assimilation cases, C1-C3, especially for $PM_{2.5}$. When the number of observation sites are decreased from 85 to 28, the RMSE in O_3 predictions increases slightly (by 13%, from 11.5 to 13.3 ppb) and RMSE in $PM_{2.5}$ increases slightly (by 42%, from 15.7 to 22.4 μg m^{-3}) but still decreased by 40% from that in CMAQ (37.3 μg m^{-3}) based on the average of all 28 cities. We note that the evaluation for C1-C3 was performed while withholding observations from the sites used for assimilation, thus implying that such improvement through assimilation also applies to the locations where air pollution is not monitored.

RSM-assimilation has advantages in cases where few observation data are available. However, since emissions are adjusted at the city level, the RSM-assimilation method has limited flexibility for adjusting spatial patterns of O_3 and $PM_{2.5}$ concentrations. The spatial distribution of emissions, which are assumed to be accurate in RSM-assimilation, might also have uncertainties that could influence the performance of assimilation in terms of representing concentration gradients. In that case, adjustment of total emissions cannot reduce the biases associated with the spatial concentration gradients, which may limit the overall performance of RSM-assimilation.

3.3 Implication of uncertainties in anthropogenic emissions

In addition to reducing the RMSE of model predictions, RSM-assimilation provides the emission ratios for five pollutants that are adjusted simultaneously during assimilation. The adjusted emission ratios provide information about potential uncertainties in anthropogenic emissions.

As shown in Figure 7, for average month values, NO_x emissions appear to be underestimated in the baseline case based on emission adjustment ratios >1 in January, April, and October. VOC emissions appear to be overestimated (adjustment ratios <1) in January and October, and SO_2 emissions are underestimated in April. The emission adjustment ratio for $pPM_{2.5}$ is the largest among all pollutants, in part due to the wider range of possible changes allowed in the RSM-assimilation. The $pPM_{2.5}$ ratio is much greater than 1 in all cases and indicates a significant underestimation, particularly in April during the dust season. The biases in assimilated concentrations generally do not reach to zero due to the limited range of emission adjustment available in RSM-assimilation. For cases that have large uncertainties in the prior emissions, the simulated concentrations cannot fully be assimilated such that predictions match the observation.

An underestimation of NO_x and SO_2 emissions is evident on both clean and polluted days. On clean days, $pPM_{2.5}$ emissions are significantly underestimated in April. On polluted days, NO_x emissions are underestimated during all seasons except summer. For all days, VOC emissions are overestimated in January and October, and SO_2 emissions are underestimated in January and April but overestimated in July and October. The adjusted emission ratio for $pPM_{2.5}$ is greater than 1 across all four months suggesting a broad underestimation of primary $PM_{2.5}$ emissions. The uncertainties of $pPM_{2.5}$ emissions may be

due to the lack of inline dust simulation over NCP domain and underestimation of wind-blown dust emissions outside of NCP [31], as such underestimation of $PM_{2.5}$ is more pronounced in April during the dust season. Also, the underestimation of primary organic aerosol and intermediate VOC emissions appears to have resulted in relatively larger low-biases of simulated organic aerosols than other components in April (see Figure S5). Although increasing the $pPM_{2.5}$ emissions is an efficient way to resolve differences between modeled and observed $PM_{2.5}$ concentrations, the emission adjustment of $pPM_{2.5}$ also likely corrects for other model limitations. The large adjustment of $pPM_{2.5}$ (by over two) suggests that other model uncertainties (e.g., aerosol-PBL dynamic interactions, chemical reaction rates, and potential missing chemical reaction pathways) could also play an important role in contributing to low biases. This is also suggested from the evaluation of $PM_{2.5}$ component concentrations which imply that potential missing chemical reaction pathways for the transition of S(IV) to S(VI) [32, 33] might contribute to the low-biases of sulfate aerosols in January and July (i.e., SO_2 concentration was overestimated but the percentage of sulfate aerosols in total $PM_{2.5}$ was underestimated, see Figure S5). Further decoupling the influence of these processes can be done using advanced machine learning technology with the inclusion of certain feature data such as meteorological variables.

4. Summary and Conclusions

In this study, we developed a new assimilation method (RSM-assimilation) that uses an emission-concentration response model for assimilating $PM_{2.5}$ and O_3 observations simultaneously. The successful application of RSM-assimilation indicates that significant improvements in the agreement of predictions and observations can be achieved solely by adjusting the emissions. For instance, the RMSE for O_3 and $PM_{2.5}$ predictions decreased by about 35% and 58%, respectively, demonstrating the effectiveness of the new assimilation method based on the emission-concentration response model. We found that the RSM-assimilation has limited ability for assimilating concentrations at the edge of the control region due to the influence of emissions from surrounding regions. Compared to $PM_{2.5}$, O_3 concentrations are harder to assimilate with the new method due in part to the larger contributions from background and natural sources. An advantage of RSM-assimilation is that it requires very little observational data, since it uses prior knowledge of the spatial distribution of emissions. Therefore the approach is most suitable for cases where few observation are available.

The RSM-assimilation also provides useful information to improve understanding of uncertainties in the emission inventory. Based on the adjusted emission ratios, we found that the NO_x emissions are likely underestimated in January, April, and October; SO_2 emissions are likely underestimated in April; NH_3 emissions are likely overestimated in April; and VOC emissions are likely overestimated in January and October. Also, $pPM_{2.5}$ emissions appear to be significantly underestimated in April during the dust season. Despite the success of the RSM-assimilation application, some limitations were identified that require future improvement. For example, due to the lack of NH_3 observations, we adjusted the NH_3 emissions simultaneously with $pPM_{2.5}$ emissions in this study. Future work can be conducted by implementing both surface measurements and satellite retrievals (e.g., NO_2, SO_2, NH_3, and HCHO) to optimize the emission accuracy across the whole domain. The

inclusion of NH_3 observations can improve the method to better constrain the adjustment for $PM_{2.5}$. Further improvement can be also done to separate the emissions by sectors with additional correction functions such as the spatial pattern of each emission category based on observations like satellites. In addition, we assumed that the emissions changes have immediate impact on $PM_{2.5}$ and O_3 concentrations, but incorporating an assimilation time window into the method is necessary to account for the time needed for pollution transport and chemical formation upwind of the monitors.

Supplementary Material

Refer to Web version on PubMed Central for supplementary material.

Acknowledgments:

The authors gratefully acknowledge the free availability and use of observation datasets. The views expressed in this manuscript are those of the authors alone and do not necessarily reflect the views and policies of the U.S. Environmental Protection Agency.

Funding: This work was supported in part by National Natural Science Foundation of China (41907190, 51861135102), and National Key R & D program of China (2018YFC0213805). This work was completed on the “Explorer 100” cluster system of Tsinghua National Laboratory for Information Science and Technology.

Annex: abbreviations in the text

CMAQ model	Community Multiscale Air Quality model
CTM	chemical transport model
DS	Downscaler
eVNA	enhanced Voronoi Neighbor Averaging
HCHO	Formaldehyde
MEGAN	Model for Emissions of Gases and Aerosols from Nature
MEIC	Multi-resolution Emission Inventory for China
NCP	North China Plain
NH_3	Ammonia
NMB	Normalized Mean Bias
NO_x	nitrogen oxides
O_3	ozone
PBL	planetary boundary layer
$PM_{2.5}$	fine particulate matter
$pPM_{2.5}$	primary fine particulate matter
R^2	R-squared

RMSE	Root Mean Square Error
RSM	response surface model
SO_2	Sulfur dioxide
VNA	Voronoi Neighbor Averaging
VOC	volatile organic compounds
WRF model	Weather Research and Forecasting model

References

1. Forouzanfar MH; Alexander L; Anderson HR; Bachman VF; Biryukov S; Brauer M; Burnett R; Casey D; Coates MM; Cohen A; Delwiche K Global, regional, and national comparative risk assessment of 79 behavioural, environmental and occupational, and metabolic risks or clusters of risks in 188 countries, 1990–2013: a systematic analysis for the Global Burden of Disease Study 2013. The Lancet, 2015, 386 (10010), 2287–2323.
2. HEI, 2019 Health Effects Institute. 2019. State of Global Air 2019 Available: www.stateofglobalair.org [accessed 08/22/2019].
3. Gold CM; Remmele PR; Roos T; 1997 Voronoi methods in GIS In: van Kreveld M; Nievergelt J; Roos T; Widmayer P (Eds.), Algorithmic Foundations of Geographic Information Systems. Lecture Notes in Computer Science Springer, Berlin, Heidelberg, pp. 21–35.
4. Ding D; Zhu Y; Jang C; Lin C-J; Wang S; Fu J; Gao J; Deng S; Xie J; Qiu X Evaluation of health benefit using BenMAP-CE with an integrated scheme of model and monitor data during Guangzhou Asian Games. J. Environ. Sci. (China) 42, 2016, 9–18. 10.1016/j.jes.2015.06.003. [PubMed: 27090690]
5. U.S.EPA, 2015 Bayesian Space-time Downscaling Fusion Model (Downscaler) Derived Estimates of Air Quality for 2011 U.S. Environmental Protection Agency, Washington, DC https://nepis.epa.gov.
6. U.S.EPA, 2016 Technical Information about Fused Air Quality Surface Using Downscaling Tool: Metadata Description U.S. Environmental Protection Agency, Washington, DC https://www.epa.gov/sites/production/files/2015-2009/documents/dsmetadataair_0612_2010.pdf.
7. Li J; Zhu Y; Kelly JT; Jang CJ; Wang S; et al. Health benefit assessment of PM2. 5 reduction in Pearl River Delta region of China using a model-monitor data fusion approach. Journal of environmental management, 2019, 233, 489–498. [PubMed: 30594114]
8. Kelly JT; Jang CJ; Timin B; Gantt B; Reff A; et al. A system for developing and projecting PM2. 5 spatial fields to correspond to just meeting National Ambient Air Quality Standards. Atmospheric Environment: X, 2019, 2, 100019. [PubMed: 31534416]
9. Lu X; Zhang S; Xing J; Wang Y; Chen W; Ding D; Wu Y; Wang S; Duan L; & Hao J Progress of Air Pollution Control in China and Its Challenges and Opportunities in the Ecological Civilization Era. Engineering, 2020.
10. Mendoza-Dominguez A; Russell AG; Iterative inverse modeling and direct sensitivity analysis of a photochemical air quality model. Environmental science & technology, 2000, 34(23), 4974–4981.
11. Miyazaki K; Eskes H; Sudo K; Boersma KF; Bowman K; and Kanaya Y Decadal changes in global surface NOx emissions from multi-constituent satellite data assimilation, Atmos. Chem. Phys, 2017, 17, 807–837, 10.5194/acp-17-807-2017.
12. Tang W; Cohan DS; Lamsal LN; Xiao X; and Zhou W Inverse modeling of Texas NOx emissions using space-based and ground-based NO2 observations, Atmos. Chem. Phys, 2013, 13, 11005–11018, 10.5194/acp-13-11005-2013.
13. Zhang L; Chen Y; Zhao Y; Henze DK; Zhu L; et al. Agricultural ammonia emissions in China: reconciling bottom-up and top-down estimates, Atmos. Chem. Phys, 2018, 18, 339–355, 2018.

14. Xing J; Wang S; Zhao B; Wu W; Ding D; et al. Quantifying nonlinear multiregional contributions to ozone and fine particles using an updated response surface modeling technique. Environmental science & technology, 2017, 51(20), 11788–11798. [PubMed: 28891287]
15. Xing J; Ding D; Wang S; Zhao B; Jang C; et al. Quantification of the enhanced effectiveness of NO x control from simultaneous reductions of VOC and NH 3 for reducing air pollution in the Beijing–Tianjin–Hebei region, China. Atmospheric Chemistry and Physics, 2018, 18(11), 7799–7814.
16. Xing J; Zheng S; Ding D; Kelly JT; Wang S; et al. Deep learning for prediction of the air quality response to emission changes. Environmental science & technology, 2020, 54(14), 8589–8600. [PubMed: 32551547]
17. Xing J; Li S; Jiang Y; Wang S; Ding D; Dong Z; Zhu Y; and Hao J Quantifying the emission changes and associated air quality impacts during the COVID-19 pandemic in North China Plain: a response modeling study, Atmos. Chem. Phys. Discuss, 2020, 10.5194/acp-2020-522, in review
18. Ding D; Xing J; Wang S; Liu K; Hao J Estimated contributions of emissions controls, meteorological factors, population growth, and changes in baseline mortality to reductions in ambient PM 2.5 and PM 2.5-related mortality in China, 2013–2017. Environmental health perspectives, 2019, 127(6), 067009.
19. Morrison H; Thompson G; Tatarskii V Impact of cloud microphysics on the development of trailing stratiform precipitation in a simulated squall line: Comparison of one- and two-moment schemes. Monthly Weather Review, 2009 137:991–1007
20. Iacono MJ; Delamere JS; Mlawer EJ; Shephard MW; Clough SA; Collins WD. Radiative forcing by long-lived greenhouse gases: Calculations with the aer radiative transfer models. Journal of Geophysical Research-Atmospheres, 2008, 113.
21. Kain JS. The kain-fritsch convective parameterization: An update. Journal of Applied Meteorology, 2004, 43:170–181.
22. Xiu AJ; Pleim JE. Development of a land surface model. Part i: Application in a mesoscale meteorological model. Journal of Applied Meteorology, 2001, 40:192–209.
23. Pleim JE. A combined local and nonlocal closure model for the atmospheric boundary layer. Part i: Model description and testing. Journal of Applied Meteorology and Climatology, 2007, 46:1383–1395.
24. Sarwar G; Luecken D; Yarwood G; Whitten GZ; Carter WPL. Impact of an updated carbon bond mechanism on predictions from the cmaq modeling system: Preliminary assessment. Journal of Applied Meteorology and Climatology, 2008, 47:3–14.
25. Appel KW; Pouliot GA; Simon H; Sarwar G; Pye HOT; Napelenok SL; et al. Evaluation of dust and trace metal estimates from the community multiscale air quality (cmaq) model version 5.0. Geoscientific Model Development, 2013, 6:883–899.
26. Li M; Zhang Q; Kurokawa J-I; Woo J-H; He K; Lu Z; et al. Mix: A mosaic asian anthropogenic emission inventory under the international collaboration framework of the mics-asia and htap. Atmospheric Chemistry and Physics, 2017, 17:935–963.
27. Guenther A; Karl T; Harley P; Wiedinmyer C; Palmer PI; Geron C Estimates of global terrestrial isoprene emissions using megan (model of emissions of gases and aerosols from nature). Atmospheric Chemistry and Physics, 2006, 6:3181–3210.
28. Ding D Response surface model of atmospheric PM2.5 and O3 concentration with precursor emissions and its application, doctoral thesis, Tsinghua University, 2020.
29. Chang X; Wang S; Zhao B; Xing J; Liu X; Wei L; et al. Contributions of inter-city and regional transport to PM2. 5 concentrations in the Beijing-Tianjin-Hebei region and its implications on regional joint air pollution control. Science of The Total Environment, 2019, 660, 1191–1200.
30. Dong Z; Wang S; Xing J; Chang X; Ding D; Zheng H Regional transport in Beijing-Tianjin-Hebei region and its changes during 2014–2017: The impacts of meteorology and emission reduction. Science of The Total Environment, 2020, 139792.
31. Xing J; Mathur R; Pleim J; Hogrefe C; Gan C-M; Wong DC; and Wei C: Can a coupled meteorology–chemistry model reproduce the historical trend in aerosol direct radiative effects over the Northern Hemisphere?, Atmos. Chem. Phys, 2015, 15, 9997–10018.

32. Fu X; Wang S; Chang X et al. Modeling analysis of secondary inorganic aerosols over China: pollution characteristics, and meteorological and dust impacts. Sci Rep, 2016, 6, 35992. [PubMed: 27782166]

33. Zhang S; Xing J; Sarwar G et al. Parameterization of heterogeneous reaction of SO2 to sulfate on dust with coexistence of NH3 and NO2 under different humidity conditions. Atmospheric Environment, 2019, 208, 133–140. [PubMed: 31186616]

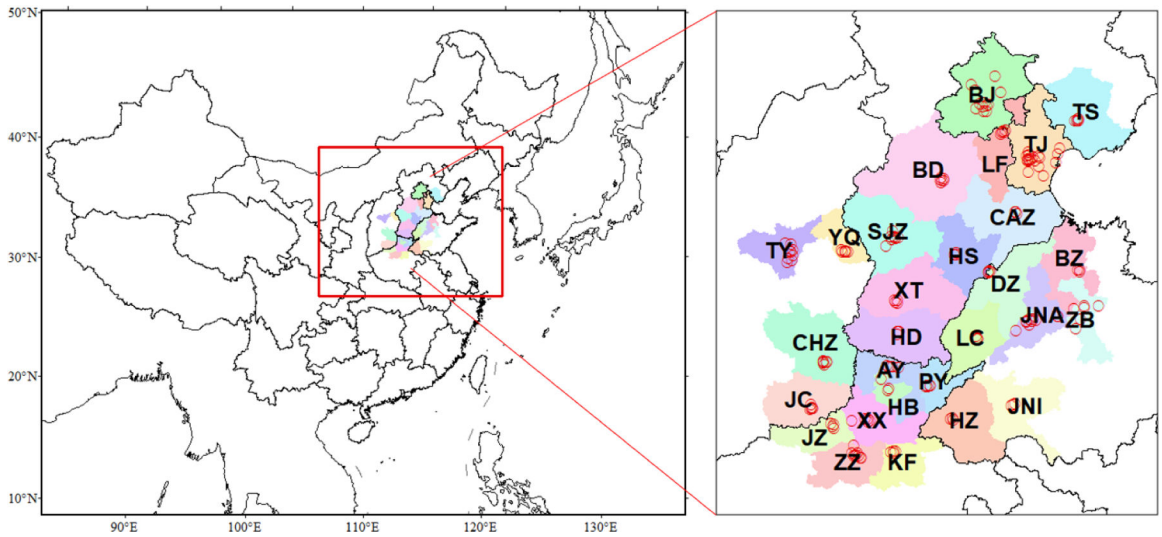

Figure 1.

Simulation domain and observation sites in 2+26 cities of North China Plain (red dots: surface monitor sites for NO_2, SO_2, O_3 and $PM_{2.5}$; the 28 cities are BJ-Beijing, TJ-Tianjin, BD-Baoding, CAZ-Cangzhou, HD-Handan, HS-Hengshui, LF-Langfang, SJZ-Shijiazhuang, TS-Tangshan, XT-Xingtai, TY-Taiyuan, YQ-Yangquan, ZZ-Zhengzhou, JZ-Jiaozuo, AY-Anyang, HB-Hebi, XX-Xinxiang, KF-Kaifeng, PY-Puyang, HZ-Heze, LC-Liaocheng, DZ-Dezhou, JNI-Jining, ZB-Zibo, JNA-Jinan, BZ-Binzhou, JC-Jincheng, CHZ-Changzhi).

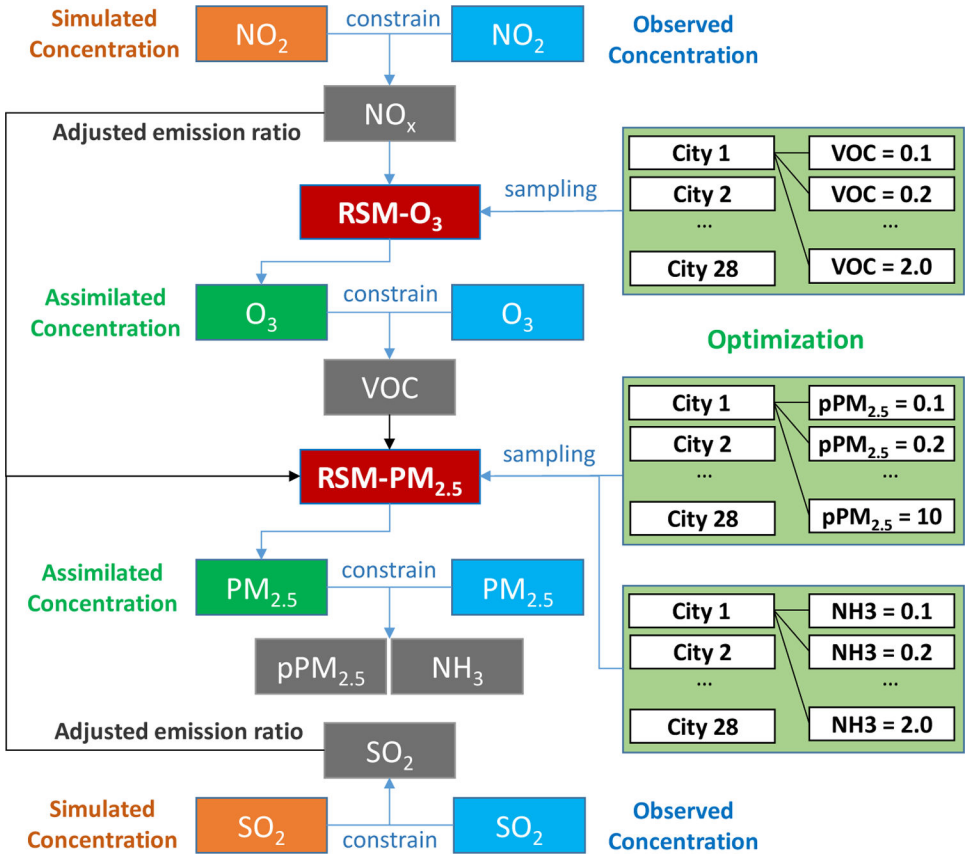

Figure 2.

The emission-concentration-based response modeling framework. (In assimilating observational data, NO_x and SO_2 emissions are adjusted first, followed by optimization for VOC and then $pPM_{2.5}$ and NH_3 emissions)

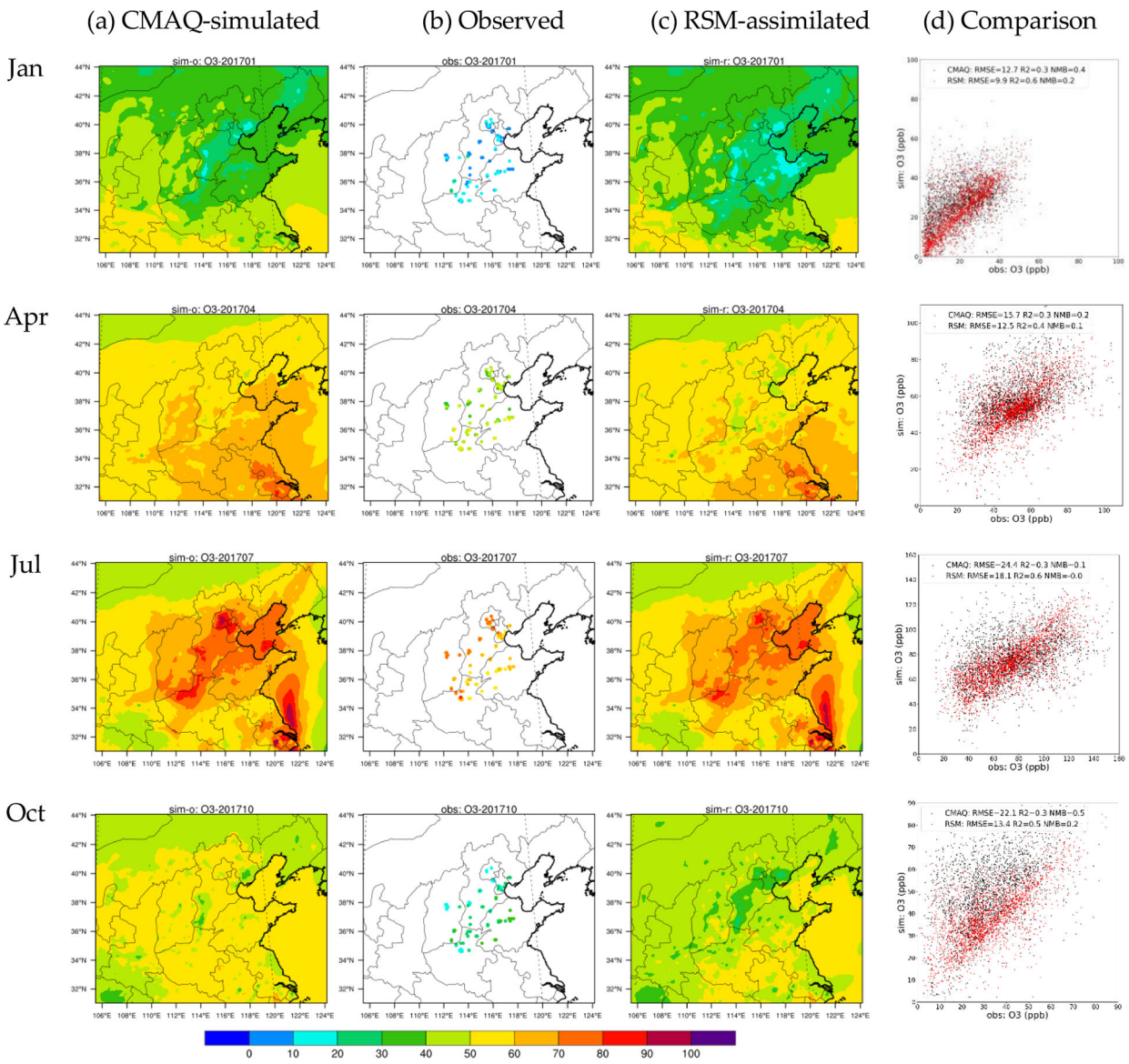

Figure 3.

Comparions of CMAQ-simulated, observed, and RSM-assimilated O_3 concentrations

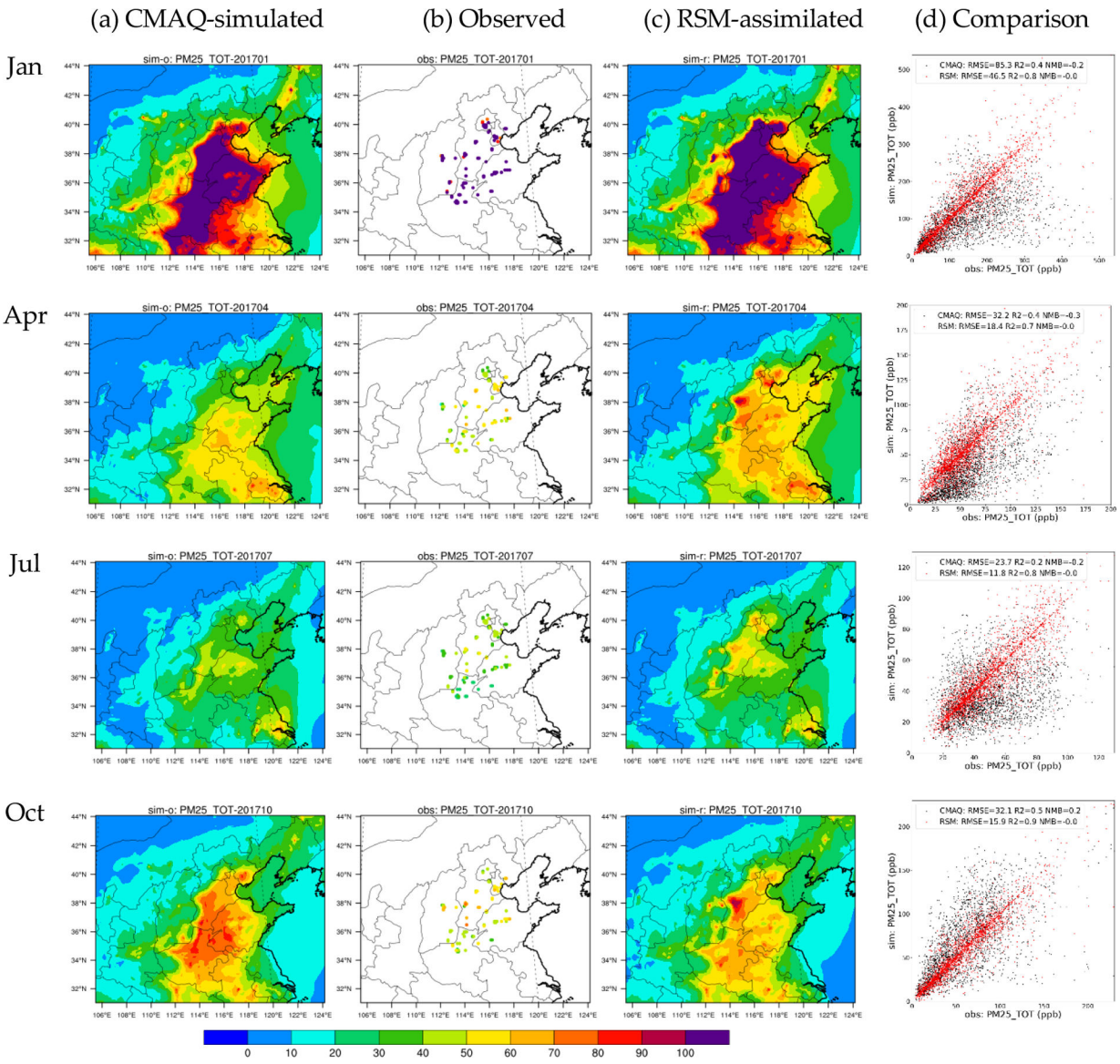

Figure 4.

Comparions of CMAQ-simulated, observed, and RSM-assimilated $PM_{2.5}$ concentrations

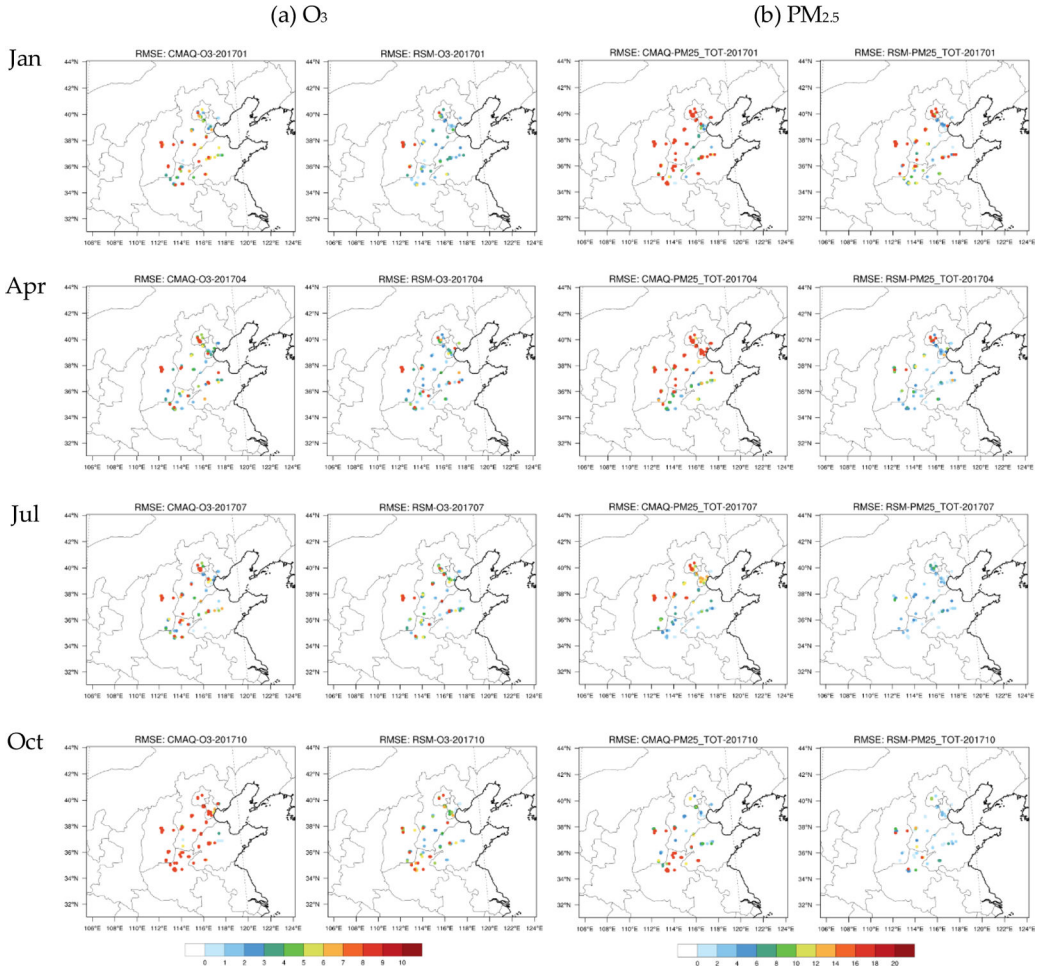

Figure 5.

Comparisons of RMSE in CMAQ-simulated and RSM-assimilated concentrations of O_3 (ppb) and $PM_{2.5}$ ($\mu g\ m^{-3}$) across all observation sites

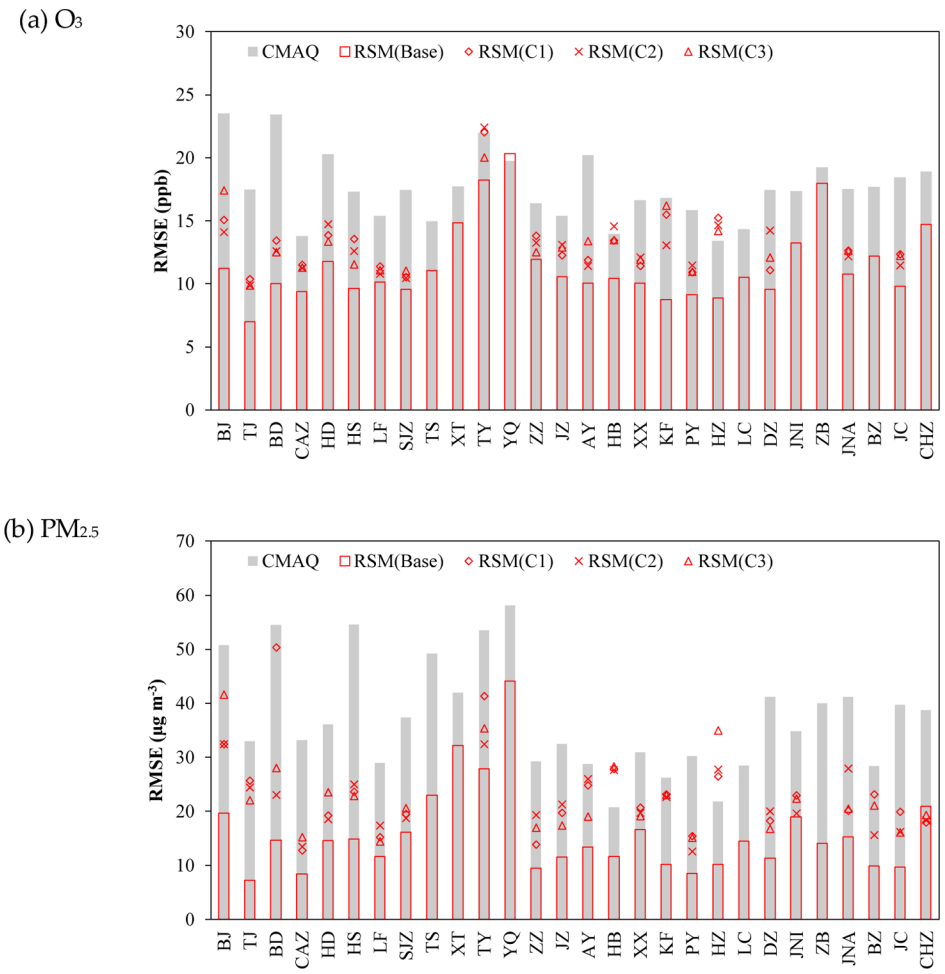

Figure 6.
The performance of RSM-assimilation by using different number of observation sites

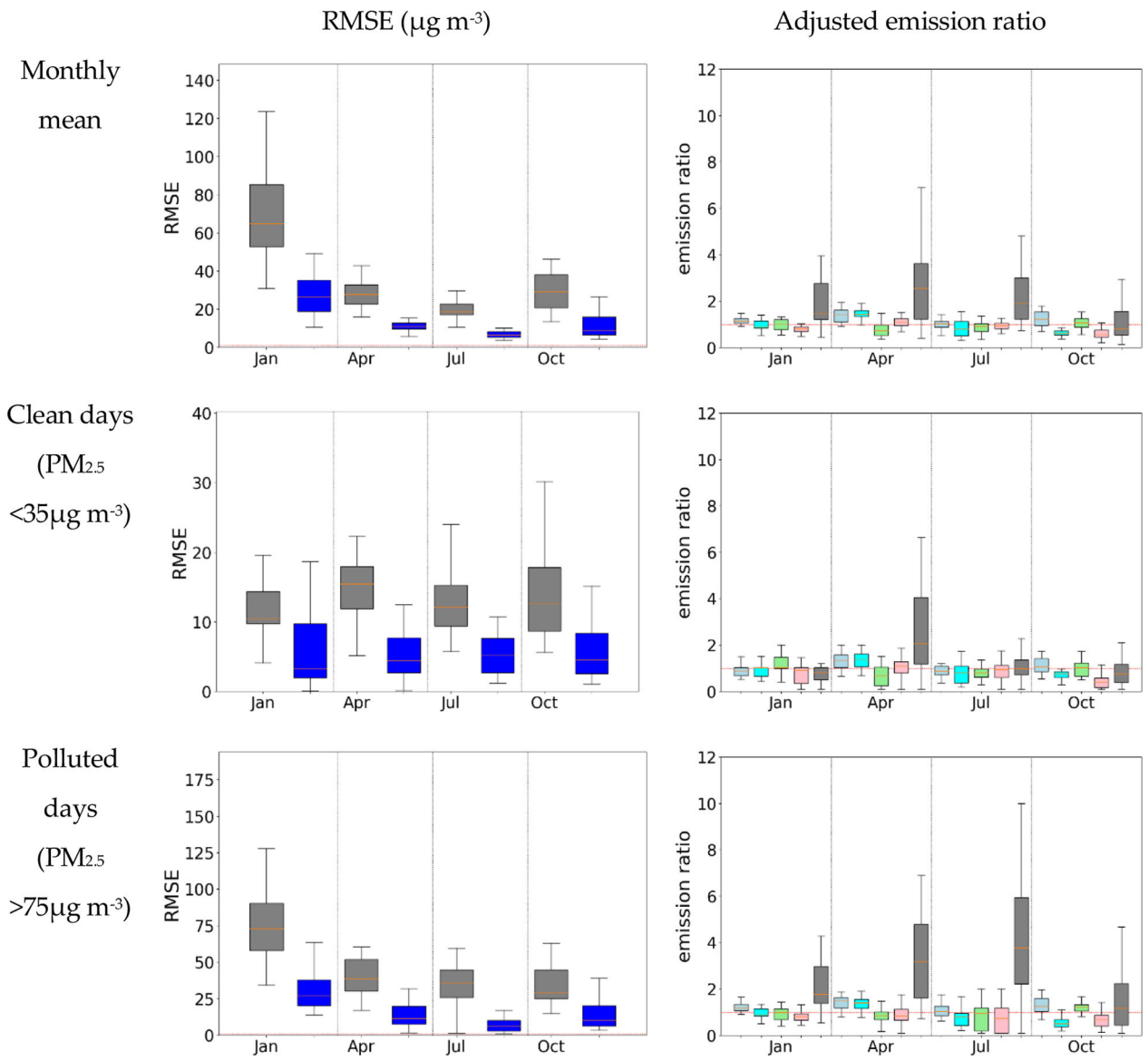

Figure 7.

The RMSE (left: grey-CMAQ; blue-RSM) and Adjusted emission ratio for the air quality assimilation (right, baseline=1. lightblue-NO_x; cyan-SO_2, green-NH_3; pink-VOC; grey-$pPM_{2.5}$) at different polluted levels